NOVEL GRAPH THEORETIC ENHANCEMENTS TO ICP-BASED VIRTUAL CRANIOFACIAL RECONSTRUCTION

A.S. Chowdhury[1], *S.M. Bhandarkar*[1], *R.W. Robinson*[1], *J.C. Yu*[2]

[1]*Department of Computer Science*
The University of Georgia
Athens, GA 30602 – 7404, *USA.*

[2]*Department of Plastic Surgery*
Medical College of Georgia
Augusta, GA 30912 – 4080, *USA.*

ABSTRACT

Novel graph theoretic enhancements to the well-known Iterative Closest Point (ICP) algorithm are proposed in the context of virtual craniofacial reconstruction. The input to the algorithm is a sequence of Computed Tomography (CT) images of a fractured human mandible. The closest set computation in the ICP algorithm is performed using the Maximum Cardinality Minimum Weight (MCMW) bipartite graph matching algorithm. Furthermore, the bounding boxes of the fracture surfaces are used to generate multiple candidate solutions based on the automorphism group of a cycle graph. The best candidate solution is selected by exploiting geometric constraints that are invariant to rigid body transformations and anatomical knowledge of the global shape of the mandible. Initialization of the ICP algorithm with the best candidate solution is found to improve surface reconstruction accuracy. Experimental results on CT scans of real patients are presented.

Keywords

Biomedical image processing, Image registration, Graph theory, Pattern matching.

1. INTRODUCTION

In modern society, craniofacial fractures are commonly encountered; the major causes are vehicle accidents, sports-related injuries and gunshot wounds [1]. The cost of surgery becomes prohibitive with the increased operating time necessary to ensure an accurate reconstruction [2]. Thus a plastic surgeon is faced with the challenging task of accurately reconstructing the fractured jaw in a limited amount of time. The Iterative Closest Point (ICP) algorithm [3] along with its problem-specific variations has been found to be useful for surface registration in medical imaging [4]. The ICP algorithm, being a local search algorithm, can generate an accurate solution, provided it is given a good starting point. Moreover, it is often imperative to incorporate geometric constraints [5] and global shape knowledge [6] to improve the accuracy of general pattern matching algorithms, including those that are used in medical image analysis. The primary contributions of the paper are the proposed graph theoretic enhancements to the conventional ICP algorithm in the context of virtual craniofacial reconstruction which include (a) computation of the closest set in the ICP algorithm using the Maximum Cardinality Minimum Weight (MCMW) bipartite graph matching algorithm [7]; (b) generation of multiple candidate transformations by exploiting the properties of the automorphism group for cycle graphs [8]; (c) subsequent selection of the best candidate solution using geometric constraints and global shape of the mandible and (d) improvement of the surface reconstruction accuracy by providing a better initialization (via steps (b) and (c)) for the conventional ICP algorithm.

2. IMAGE PREPROCESSING

The input to the computer vision-guided virtual craniofacial reconstruction system is a sequence of 2-D grayscale images of a fractured human mandible, generated via Computed Tomography (CT). Although the bone fragments and soft tissue possess very different intensity values, components with intensities similar to those of the mandible fragments, and the overall inhomogeneity of the intensity field, preclude us from using a good fixed threshold. Entropy based thresholding [9] is hence employed to segment the broken bone. For an image, the entropy S_c, for each class c (which comprises of several graylevels) can be computed using the grayscale histogram as follows:

$$S_c = \sum_{k \in G_c} p(k) \log_2(p(k)) \quad (1)$$

where $p(k)$ is the probability of a pixel having a grayscale value k and G_c is the set of graylevels for class c. In the context of binarization (where $c = 1, 2$), the graylevel threshold T is chosen such that the total entropy $S = S_1 + S_2$ is maximized. Subsequently, a 2-D Connected Component Labeling (CCL) procedure in conjunction with a component area filter is employed to remove undesired artifacts which are typically small in size. A 3-D component representing a fractured jaw bone is identified by computing the area of overlap of the corresponding 2-D components in successive 2-D CT image slices. There are two such broken fragments in the present CT scans, and we denote them as frg_1 and frg_2. The interesting points on a fracture contour (typically points of high curvature) are manually extracted in each 2-D CT image slice. The fracture contour points from the entire CT image stack are then collated to generate the 3-D surface point dataset. A 3-D surface point dataset is generated for each fracture surface.

3. FRACTURE SURFACE REGISTRATION USING THE ICP ALGORITHM

The fracture surface pairs are first registered using the ICP algorithm described in [3] with the incorporation of a novel graph-theoretic enhancement. The main steps in the enhanced ICP algorithm [10] are as follows:

1. The matching points in one fracture surface data set, called the model data set, that correspond to points in the other fracture surface data set, called the sample data set, are determined and termed the *closest set*. The matching point pairs

are determined using the MCMW bipartite graph matching algorithm [7]. The use of the MCMW graph matching algorithm obviates the need for any prior alignment of the two fracture surface data sets when computing the *closest set* in the ICP algorithm. The sample data set and model data set are represented by the two disjoint vertex sets V_{1B} and V_{2B} (where $|V_{1B}| \neq |V_{2B}|$) respectively in the bipartite graph $G_B(V_{1B} \cup V_{2B}, E_B)$. The edge-weight $w_{i,j}$ of the edge $e_{i,j} \in E_B$ joining the two vertices v_i and v_j (such that $v_i \in V_{1B}$ and $v_j \in V_{2B}$) is chosen to be the Euclidean distance between the vertices. Note that the Euclidean distance measure is invariant under a 3-D rigid body transformation. Thus, the edge weight is given by:

$$w_{i,j} = ((x_i - x_j)^2 + (y_i - y_j)^2 + (z_i - z_j)^2)^{1/2} \quad (2)$$

The MCMW algorithm for a bipartite graph has a time complexity of $O(n^3)$ [7], where $n = \max\{|V_{1B}|, |V_{2B}|\}$.

2. The 3-D rigid body transformation, computed using the closest set, is applied to the original sample data set. The Mean Squared Error (MSE) between the transformed sample data points and the corresponding closest points is given by:

$$\epsilon^2 = (1/p)\sum_{i=1}^{p}((c_i - (Rs_i + T))^2) \quad (3)$$

where R denotes the rotation matrix, T denotes the translation vector, s_i denotes a point in the sample data set, c_i represents the corresponding point in the closest set and $p = \min\{|V_{1B}|, |V_{2B}|\}$.

4. GENERATION OF MULTIPLE CANDIDATE SOLUTIONS

Besl and McKay [3] propose using multiple initial states as means to attain a global minimum in their version of the ICP algorithm [3]. They suggest comparing the shape-based principal moments and sampling the quaternion states based on rotation groups of regular polyhedra to produce these multiple initial starting states [3]. We choose to generate multiple solutions, one of which is eventually used as the starting point for the ICP algorithm, based on the automorphism group of a fracture surface bounding box which is modeled as a cycle graph. The bounding box for individual fracture surfaces is simply constructed using two pairs of extreme points of a fracture contour that appear in the first and last image slice of the CT image sequence and is modeled as a cycle graph of order 4. The weights assigned to the edges of the cycle graph are the Euclidean distances between the corresponding points. Let us denote the cycle graph of the fracture surface of the fragment frg_1 by B_1 and that of frg_2 by B_2. The main idea is that if the two fracture surfaces are well matched, then their bounding boxes are also well matched. We use the following interesting concepts from graph isomorphism and graph automorphism in this connection [8]:

Definition 1 *Two graphs $G_1 = (V_1, E_1)$ and $G_2 = (V_2, E_2)$ are isomorphic, denoted by $G_1 \cong G_2$, if there exists a bijection $M \subseteq V_1 \times V_2$ such that, for every pair of vertices $v_i, v_j \in V_1$ and $w_i, w_j \in V_2$ with $(v_i, w_i) \in M$ and $(v_j, w_j) \in M$, $(v_i, v_j) \in E_1$ if and only if $(w_i, w_j) \in E_2$. In such a case M is a graph isomorphism from G_1 to G_2.*

Definition 2 *An automorphism of a graph G is a graph isomorphism between G and itself.*

The set of all automorphs of a graph forms a group under the operation of composition. This group is termed the *automorphism group* of the graph.

Lemma 1 *The automorphism group of a cycle graph C_n on $n \geq 3$ vertices is a group of order $2n$.*

Proof: A cycle graph with C_n on $n \geq 3$ vertices is characterized by exactly n rotations as well as exactly n reflections. Thus, the resulting automorphism group has order $2n$.

Thus the automorphism group of, say, B_2 consists of 4 rotation members and 4 reflection members. This means that there can be 8 possible competing orientations of B_2 that match with B_1. We denote the l^{th} automorph of B_2 by $AB_{2,l}$.

5. SELECTION OF BEST POSSIBLE CANDIDATE SOLUTION

Note that the MCMW bipartite graph matching algorithm essentially establishes the correspondence between points on the two opposable fracture surfaces. Our goal, in this paper, is to employ additional constraints, specifically geometric constraints and global shape knowledge to improve the results of surface registration.

5.1. Filtering based on Geometric Constraints

Kim and Kak [5] have shown how local geometric constraints can be exploited to improve the correspondence in the context of object recognition. We introduce a dissimilarity function based on two geometric constraints which are invariant to rigid body transformation. In order for B_1 and $AB_{2,l}$ to be well matched:

1. The lengths of corresponding pairs of sides of B_1 and $AB_{2,l}$ should be well matched. Let us denote the lengths of the i^{th} sides of B_1 and $AB_{2,l}$ by d_i^1 and $d_i^{2,l}$ respectively.
2. The angles between the corresponding pairs of sides of B_1 and $AB_{2,l}$ should also be well matched. Let us denote the angle bounded by sides i and j of B_1 and $AB_{2,l}$ by $\theta_{i,j}^1$ and $\theta_{i,j}^{2,l}$ respectively.

The dissimilarity function $\Gamma(B_1, AB_{2,l})$ between B_1 and the l^{th} member of AB_2 can now be defined as a linear combination of the above factors:

$$\Gamma(B_1, AB_{2,l}) = \lambda_1\Gamma_1(B_1, AB_{2,l}) + \lambda_2\Gamma_2(B_1, AB_{2,l}), \text{ where}$$

$$\Gamma_1(B_1, AB_{2,l}) = \textstyle\sum_{i=1}^{4}(|d_i^1 - d_i^{2,l}|), \text{ and}$$

$$\Gamma_2(B_1, AB_{2,l}) = \textstyle\sum_{i=1}^{4}(|\theta_{i,((i \bmod 4)+1)}^1 - \theta_{i,((i \bmod 4)+1)}^{2,l}|) \quad (4)$$

The normalized values of λ_1 and λ_2 (such that $\lambda_1 + \lambda_2 = 1$) are determined from the variance of the values of the terms $\Gamma_1(B_1, AB_{2,l})$ and $\Gamma_2(B_1, AB_{2,l})$ for 8 possible values of l. The dissimilarity function is computed between B_1 and each of the automorphs of AB_2. The lower the value of the dissimilarity function $\Gamma(B_1, AB_{2,l})$, the better the match between B_1 and $AB_{2,l}$. The 8 automorphs are ranked in ascending order of their $\Gamma(B_1, AB_{2,l})$ values and the first 4 automorphs are chosen as the more suitable candidates for being opposable to B_1.

5.2. Filtering based on Global Shape Knowledge

After the 4 eligible members (yielding the 4 low $\Gamma(B_1, AB_{2,l})$ values) are determined, the 4 transformations $(\phi_1, \cdots, \phi_4)$ are estimated between B_1 and the eligible automorphs. Each of these four transformations is applied to frg_1 to register it to frg_2. Wang et al. [6] use geodesics and local geometry to improve the surface correspondence. We exploit the knowledge of the global shape of the human mandible to disambiguate between the 4 reconstructed mandibles by comparing each of them with an intact reference mandible using a suitable shape similarity measure. The contours $Co_1, \cdots, Co_4$ of each of the reconstructed mandibles and contour Co_{ref} of the intact reference mandible are extracted using simple edge detection. Contour-based shape similarity measures have been well explored in the computer vision literature (e.g., see [11]). We choose Hausdorff distance to compute the similarity measure because of its relatively low $O(n^2)$ time complexity and because it obviates the need to establish prior correspondence between pixels on the two contours under consideration. The bounding box for each of the five contours is determined. Each contour is scaled to make its bounding box exactly fit to the input image. The Contour Hausdorff Distance (CHD) [12] between two scaled contour data sets Co_i (where $i = 1, \cdots, 4$) and Co_{ref} is given by:

$$H(Co_i, Co_{ref}) = \max(h(Co_i, Co_{ref}), h(Co_{ref}, Co_i)) \quad (5)$$

where $h(Co_i, Co_{ref})$ is the directed Hausdorff distance between the two data sets Co_i and Co_{ref} and is defined as:

$$h(Co_i, Co_{ref}) = \max_{a \in Co_i} \min_{b \in Co_{ref}} ||a - b|| \quad (6)$$

Here $||a - b||$ represents the Euclidean distance between the points a and b. The contour Co^* that yields the minimum value of CHD is deemed to be the best matching contour and the corresponding transformation ϕ^* is treated as the best initial state of the ICP algorithm. We term the above coarse registration approach as the *Geometric* algorithm.

6. HYBRID GEOMETRIC-ICP ALGORITHM

The transformation ϕ^*, the output of the Geometric algorithm, is used as the initial transformation for the ICP algorithm. The ICP algorithm initialized with ϕ^*, is denoted as the *Geometric-ICP* algorithm, The transformation ϕ_{GICP} of the Geometric-ICP algorithm can be also interpreted as the following composite transformation:

$$[\phi_{GICP}] = [\phi^*][\phi_{ICP}] \quad (7)$$

where ϕ_{ICP} denotes the transformation obtained from the ICP algorithm. We also measure the MSE resulting from the best possible coarse registration transformation ϕ^* computed using the Geometric algorithm. Note that although the Geometric algorithm exploits geometric constraints and knowledge of global shape it uses only 4 pairs of corresponding points and lacks iterative refinement capability.

7. EXPERIMENTAL RESULTS

In this section, we show the results of image preprocessing, generation of multiple candidate solutions and image registration. Details of experimental results are limited to a single case in the interest of brevity. In Figure 1, a CT image sequence of a fractured human mandible is displayed. The bone components clearly display higher grayscale values compared to the soft tissue and artifacts. The effect of image processing on a typical CT image slice is

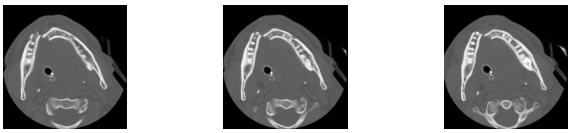

Fig. 1. CT Image Sequence of a Fractured Human Mandible.

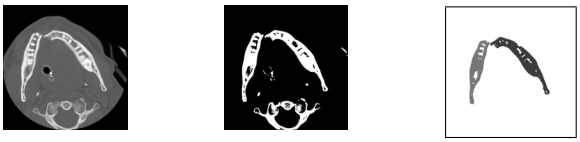

Fig. 2. Result of Image Preprocessing on a CT Image Slice.

shown in Figure 2. The middle image shows the result of entropy-based thresholding, where as the rightmost figure shows the effect of CCL and area based filtering. Note that precisely two mandibular fragments are obtained after the image preprocessing operations. The bounding boxes (B_1, B_2) of the two fracture surfaces and the automorphism group AB_2 of B_2 are determined next. The best 4 out of a total 8 competing automorphs from AB_2 are selected based on the dissimilarity function value (see Table 1) using equation (4). The best 4 candidate transformations $\phi_1, \cdots, \phi_4$ are then estimated from B_1 and the best four automorphs and applied to frg_1 resulting in the 4 reconstructed mandibles $M_1, \cdots, M_4$. Figure 3 shows the reference contour Co_{ref} and the contours of the four registered

Table 1. Dissimilarity Function Values for Competing Automorphs

Rank of the Automorph	Dissimilarity Function Value
1	52.20
2	57.30
3	61.37
4	66.51

Table 2. CHD Values for Competing Contours

Contour from Figure 3	Rank	CHD Value
Co_1	1	111.22
Co_2	2	2.24
Co_3	3	52.43
Co_4	4	149.97

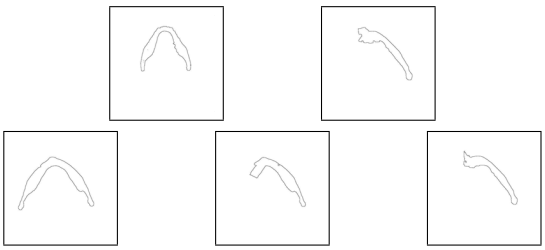

Fig. 3. Reference and Candidate Contours

mandibles $Co_1, \cdots, Co_4$ (from left to right, top to bottom respectively). Table 2 shows the CHD values obtained using equation (5), from which Co^* (equal to Co_2 in the present case) and ϕ^* (equal to ϕ_2) are estimated. Table 1, Table 2 and Figure 3 clearly demonstrate how multiple competing fracture surfaces and hence multiple candidate solutions are generated and the best (coarse) solution (denoted by ϕ^*) is obtained. Figure 4 displays the reconstruction

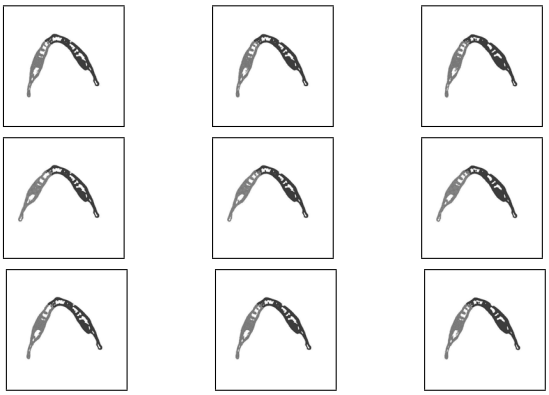

Fig. 4. Reconstruction using the ICP (row 1), Geometric (row 2) and Geometric-ICP (row 3) algorithms

Table 3. MSE Values for the Three Reconstruction Approaches

Algorithm	Transformation	MSE Value (mm^2)
ICP	ϕ_{ICP}	2.07
$Geometric$	ϕ^*	4.57
$Geometric - ICP$	ϕ_{GICP}	1.96

results for three consecutive 2-D slices using the ICP (row 1), Geometric (row 2) and Geometric-ICP (row 3) algorithms. Table 3, showing the registration accuracy of each of the three approaches, justifies the proposition of the Geometric-ICP algorithm. Since all the three reconstruction algorithms use same contour data as input; it is expected that the variability introduced by the manual extraction of high-curvature contour points does not affect the comparative reconstruction performance. For the class of fractures addressed in this paper, the surface deformation appears to be negligible, so that MSE is an acceptable figure of merit.

8. CONCLUSIONS AND FUTURE WORK

Two potential graph-theoretic enhancements to the ICP-based surface registration algorithm were discussed in this paper. First, the MCMW bipartite graph matching was used to determine the closest set in the ICP algorithm. Second, the best possible initial state, obtained from a set of candidate solutions using 3-D rigid body transformation-invariant geometric constraints, global shape knowledge and graph automorphism, was provided to the ICP algorithm. The ICP algorithm, enhanced with suitable initialization, was shown to improve the surface registration accuracy. From the perspective of an important biomedical imaging application, a novel, fast (the algorithms take less than a minute on an 1.73 GHz $Intel^{©}$ $Pentium^{©}$ M processor) yet accurate virtual reconstruction is achieved in the context of mandibular fracture reconstruction.

One direction for future work is to strengthen the geometric constraints by replacing the bounding box with the bounding cycle of a convex hull. As a graph, this bounding cycle would be an n-cycle for some n, possibly > 4. For $n > 4$, the $2n$ automorphs would provide a greater number of potential matches for the opposing fracture surface. This extension could be very useful for solving the critical correspondence problem, especially when a broken fragment is reflected or considerably rotated, as may very well be the case in a multi-fracture scenario. We also plan to explore volumetric shape matching [10] for determining the best coarsely registered mandible and the global shape (in particular, knowledge of symmetry) in the final phase of registration.

9. REFERENCES

[1] R.E. King, J.M. Scianna and G.J. Petruzzelli, "Mandible fracture patterns: a suburban trauma center experience", *Amer. Jour. Otolaryngology*, 25(5): pp. 301-307, 2004.

[2] C. Zahl, D. Muller, S. Felder and K.L. Gerlach, "Cost of miniplate osteosynthesis for treatment of mandibular fractures: a prospective evaluation", *Gesundheitswesen*, 65(10): pp. 561-565, 2003.

[3] P.J. Besl and N.D. McKay, "A Method for Registration of 3-D Shapes", *IEEE Trans. on Pat. Anal. and Mach. Intel.*, 14(2): pp. 239-256, 1992.

[4] S. Granger, X. Pennec, and A. Roche, "Rigid Point-Surface Registration Using an EM variant of ICP for Computer Guided Oral Implantology", *Proc. of the Fourth Int. Conf. on Medical Image Computing and Computer Assisted Intervention (MICCAI)*, LNCS Vol. 2208, pp. 752-761, Utretcht, The Netherlands. 2001.

[5] W. Kim and A.C. Kak, "3-D Object Recognition Using Bipartite Matching Embedded in Discrete Relaxation", *IEEE Trans. on Pat. Anal. and Mach. Intel.*, 13(3): pp. 224-251, 1991.

[6] Y. Wang, B. Peterson and L. Staib, "Shape-based 3-D Surface Correspondence Using Geodesics and Local Geometry", *Proc. of the First IEEE Int. Conf. on Computer Vision and Pattern Recognition (CVPR)*, Vol. II, pp. 644- 651, Hilton Head Island, SC. 2000.

[7] Christofides N., *Graph Theory. An Algorithmic Approach*, Academic Press, NY, 1975.

[8] Valiente G., *Algorithms on Trees and Graphs*, Springer-Verlag, Berlin-Heidelberg, 2002.

[9] P.K. Sahoo, S. Soltani, K.C. Wong and Y.C. Chen, "A Survey of Thresholding Techniques", *Computer Vision, Graphics, and Image Processing*, 41: pp. 233-260, 1988.

[10] A.S. Chowdhury, S.M. Bhandarkar, R.W. Robinson and J.C. Yu, "Virtual Craniofacial Reconstruction from Computed Tomography Image Sequences Exhibiting Multiple Fractures", *Proc. of the Thirteenth IEEE Int. Conf. on Image Processing (ICIP)*, pp. 1173-1176; Atlanta, GA. 2006.

[11] R. C. Veltkamp and L. J. Latecki, "Properties and Performance of Shape Similarity Measures", *Proc. of Tenth IFCS Intl. Conf. Data Science and Classification*, pp. 1-9, Ljubljana, Slovenia. 2006.

[12] D.P. Huttenlocher, G.A. Klanderman and W.J. Rucklidge, "Comparing Images Using the Hausdorff Distance", *IEEE Trans. on Pat. Anal. and Mach. Intel.*, 15(9), pp. 850-863, 1993.